Geophysical Research Letters

RESEARCH LETTER
10.1029/2022GL098509

Key Points:

- We extract stable station-station body-wave correlation functions using seismic energy generated by freight trains
- We perform 10-year seismic velocity monitoring around the San Jacinto Fault and observe a 2-month-long velocity perturbation in 2014
- We interpret this velocity change as caused by a previously unreported slow-slip event at the southern edge of the Anza seismic gap

Supporting Information:

Supporting Information may be found in the online version of this article.

Correspondence to:

Y. Sheng,
yixiao.sheng@univ-grenoble-alpes.fr

Citation:

Sheng, Y., Mordret, A., Sager, K., Brenguier, F., Boué, P., Rousset, B., et al. (2022). Monitoring seismic velocity changes across the San Jacinto Fault using train-generated seismic tremors. *Geophysical Research Letters*, *49*, e2022GL098509. https://doi.org/10.1029/2022GL098509

Received 2 MAR 2022
Accepted 18 SEP 2022

Author Contributions:

Conceptualization: F. Brenguier, P. Boué, F. Vernon, Y. Ben-Zion
Data curation: A. Mordret, F. Brenguier, F. Vernon, Y. Ben-Zion
Formal analysis: Y. Sheng, K. Sager, B. Rousset, Q. Higueret
Funding acquisition: F. Brenguier
Investigation: Y. Sheng, K. Sager
Methodology: Y. Sheng, A. Mordret, K. Sager, F. Brenguier, P. Boué
Resources: F. Brenguier
Software: Y. Sheng, A. Mordret
Supervision: A. Mordret, F. Brenguier, P. Boué, F. Vernon, Y. Ben-Zion

Monitoring Seismic Velocity Changes Across the San Jacinto Fault Using Train-Generated Seismic Tremors

Y. Sheng[1], A. Mordret[1], K. Sager[2], F. Brenguier[1], P. Boué[1], B. Rousset[1,3], F. Vernon[4], Q. Higueret[1], and Y. Ben-Zion[5]

[1]University Grenoble Alpes, University Savoie Mont Blanc, CNRS, IRD, University Gustave Eiffel, Grenoble, France, [2]Department of Earth, Environmental and Planetary Sciences, Brown University, Providence, RI, USA, [3]Institut Terre et Environnement de Strasbourg, Université de Strasbourg, Strasbourg, France, [4]Institute of Geophysics and Planetary Physics, University of California, San Diego, La Jolla, CA, USA, [5]Department of Earth Sciences and Southern California Earthquake Center, University of Southern California, Los Angeles, CA, USA

Abstract Microseismic noise has been used for seismic velocity monitoring. However, such signals are dominated by low-frequency surface waves that are not ideal for detecting changes associated with small tectonic processes. Here we show that it is possible to extract stable, high-frequency body waves using seismic tremors generated by freight trains. Such body waves allow us to focus on small velocity perturbations in the crust with high spatial resolution. We report on 10 years of seismic velocity temporal changes at the San Jacinto Fault. We observe and map a two-month-long episode of velocity changes with complex spatial distribution and interpret the velocity perturbation as produced by a previously undocumented slow-slip event. We verify the hypothesis through numerical simulations and locate this event along a fault segment believed to be locked. Such a slow-slip event stresses its surroundings and may trigger a major earthquake on a fault section approaching failure.

Plain Language Summary We turn seismic noise generated by freight trains into repeatable measurements of body waves that dive through the core of the San Jacinto Fault zone, CA. These body waves, which are typically hard to extract with standard approaches, are used to continuously monitor seismic velocity changes potentially associated with fault movements. During the 10-year monitoring period, we observe a 2-month-long velocity perturbation in 2014 near the Anza seismic gap. We interpret this seismic velocity change as the result of a previously unknown slow-slip event that occurred at the southern end of the seismic gap, at the transition to the very seismically active area. This slow-slip event is below the geodetic detection threshold but increases the seismic stress in the seismic gap large enough to possibly trigger a big earthquake.

1. Introduction

Fault zones release elastic energy stored in the Earth's crust by tectonic stresses in different ways. The energy release can happen rapidly and dramatically during earthquakes or gradually and aseismically during slow-slip events (SSEs) (Kato & Ben-Zion, 2021). SSEs that occur along active faults can represent a large portion of the slip budget (Peng & Gomberg, 2010), and their occurrence has also been recognized as a potential driving mechanism for major earthquakes (Kato & Ben-Zion, 2021; Radiguet et al., 2016). Despite the substantial improvements in geodetic observations, noise levels prevent the detection of small SSEs, impeding the ability to describe the complete spectrum of transient slips and their roles in earthquake cycles.

Seismic velocities are sensitive to perturbations associated with earthquakes, such as damage caused by severe shaking or post-seismic deformation (Brenguier et al., 2008). Velocity changes manifest as travel-time variations among repeating signals, and their monitoring to provide a proxy for perturbations preceding large earthquakes remains a long-sought-after goal in seismology (Niu et al., 2008). The investigation of temporal changes of seismic velocity at crustal depths is hindered by the requirement for powerful and recurrent seismic sources that act over years. Low-frequency ocean-generated surface waves (0.1–1.0 Hz) have been used to study the responses of the Earth's crust to earthquakes (Brenguier et al., 2008) and volcanoes (Brenguier et al., 2014). However, the non-localized sensitivity of long-period surface waves limits the detection of strain transients associated with small deformations and the location of the origins of the related velocity perturbations.

Validation: Y. Sheng
Visualization: Y. Sheng, A. Mordret, F. Brenguier, P. Boué
Writing – original draft: Y. Sheng
Writing – review & editing: Y. Sheng, A. Mordret, K. Sager, F. Brenguier, P. Boué, B. Rousset, F. Vernon, Q. Higueret, Y. Ben-Zion

In this study, we apply a novel approach referred to as long-base seismic interferometry, which uses correlations of anthropogenic seismic sources (e.g., freight trains) between sensors to retrieve compressional seismic body waves (*P*-waves) (Brenguier et al., 2019). Instead of using low-frequency surface waves or scattered waves to measure time-lapse travel-time perturbations (*dt*), we use high-frequency ballistic *P*-waves (>1 Hz) that travel down to a few kilometers in depth. These signals provide high sensitivity to velocity perturbations along the propagation path (sensitivity kernel in Figure 1) and reduced sensitivity to near-surface environmental processes (Clements & Denolle, 2018), enabling a close monitoring of fault zone perturbations.

2. Analyses and Observations

We focus on the Anza seismic gap, a 20-km section of the San Jacinto Fault in Southern California, USA. This seismic gap is bounded by two seismically active regions: the Hot Springs area to the north and the Trifurcation area to the south. The observed high strain rates (Johnson et al., 1994) and the absence of seismicity suggest that the Anza section is locked and can potentially host a magnitude 6.5+ earthquake (Sanders & Kanamori, 1984). Paleoseismic studies have estimated the recurrence interval of large earthquakes to be 254 ± 120 years (Rockwell et al., 2015) and indicated that the fault segment near Anza has not ruptured for more than 200 years. This area is densely equipped with geophysical instruments, making it an ideal natural laboratory for seismological research.

Train tremors excited in the nearby Coachella Valley have previously been considered a nuisance (Inbal et al., 2018); following recent studies (Brenguier et al., 2019; Pinzon-Rincon et al., 2021), we turn train tremors into a valuable source of information. The Piñon Flat Observatory is used as the anchor site, where permanent seismic stations are accompanied by a temporary nodal array (network code 9K) for tracking moving trains and examining the feasibility of retrieving body waves in correlation functions. The temporary array was in operation for about 20 days in 2018. The main processing steps are illustrated schematically in Figure 1. First, the time intervals when freight trains pass by the study area are defined. Seismic interferometry is then performed by focusing on the train tremors to construct station–station correlation functions containing high-frequency

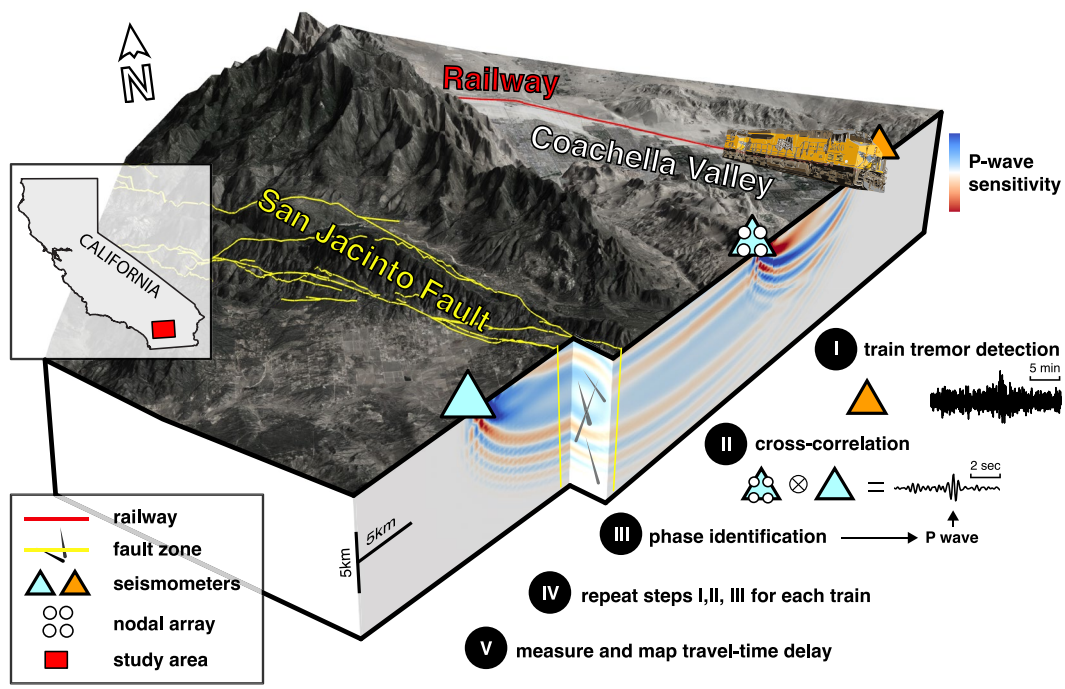

Figure 1. Schematic illustration of the location and layout of the study site and the data processing. Station–station correlation functions are repeatedly constructed using the seismic energy generated by freight trains. The compressional seismic body waves (*P*-waves) are used in the correlation functions to monitor the San Jacinto Fault Zone continuously. The *P*-wave sensitivity indicates where perturbations at depth can change the arrival times of interest. Increasing (decreasing) the velocity in the blue (red) zones leads to earlier arrivals of the compressional waves in the correlation functions. The main processing steps are explained in detail in the main text.

P-waves. Finally, the long-term travel-time perturbations of the reconstructed *P*-waves are estimated. Only the vertical component is used in this study. The detailed procedures are described further in the Supporting Information. The obtained station–station correlation functions show stable *P*-wave energy (Figure S5 in Supporting Information S1) suitable for studying seismic velocity changes. Figure 2 presents an example data set obtained from station pair II.PFO–AZ.FRD.

The analysis indicates a permanent velocity change in 2014 that lasted about two months. Such a velocity change differs from either coseismic velocity drop followed by a long-term velocity recovery (Brenguier et al., 2008), or environmental perturbations typically presenting a periodic pattern (Clements & Denolle, 2018). Intriguingly, some station pairs show positive travel-time shifts corresponding to velocity drops, while others are negative, representing velocity increases (Figure 3). We fit a step function in the least-square sense for each pair of stations to quantify the travel-time change offset (Δt) and its uncertainty in early 2014. Figure 2b illustrates the estimation for station pair II.PFO–AZ.FRD, and Figure 3c presents the results for every station pair.

There are no reports of changes to the railway system during this period. Theoretically, source changes lead to the same polarity changes of Δt for all station pairs, which is not observed. To further demonstrate that train-related changes do not induce the observed travel-time offset, the travel-time perturbation is also measured on the station pair CI.IDO–CI.BEL, following the same procedure. These stations (Figure 3b and Figure S2 in Supporting Information S1) are in the vicinity of the Joshua Tree National Park, on the other side of the railway from the San Jacinto Fault zone, more than 40 km away from the Anza seismic gap. No evident Δt was observed between these two stations in early 2014 (Figure 3). We, therefore, argue that the travel-time offsets are related to genuine seismic velocity changes near the Anza area. Environmental variations, such as groundwater level changes, can also alter seismic velocity (Clements & Denolle, 2018) in shallow structures; however, no significant precipitation was reported in the Anza region. In addition, body-wave correlation functions are less susceptible to the perturbations near the Earth's surface, suggesting the possible cause of the velocity variation occurs at depth.

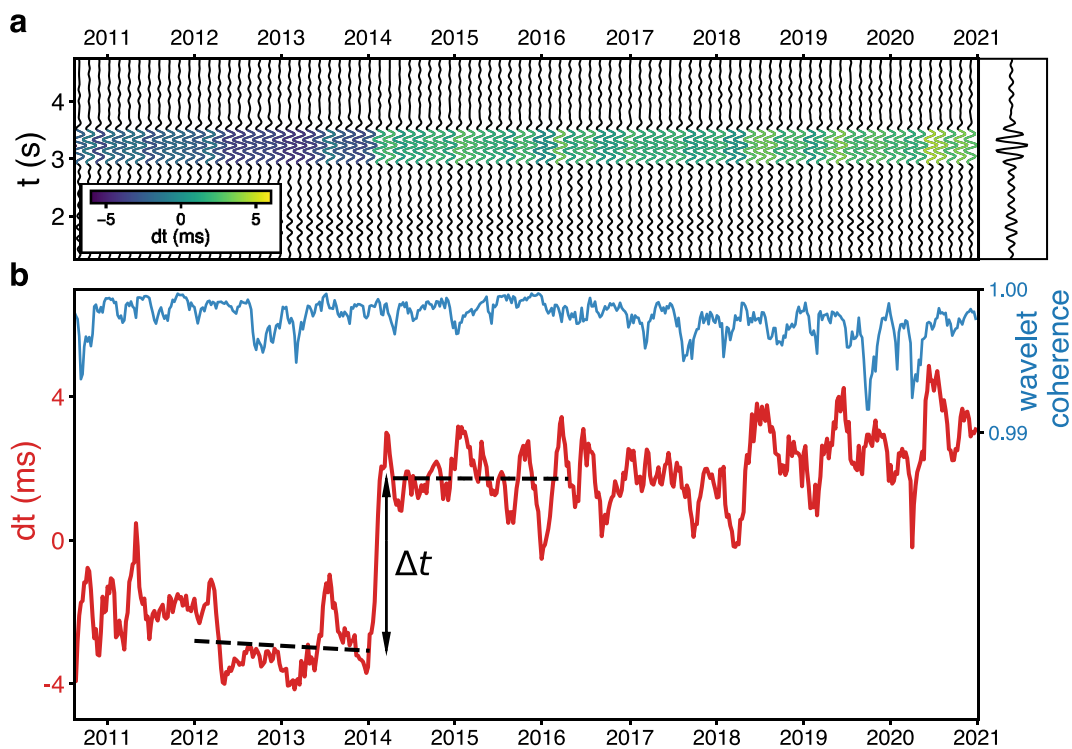

Figure 2. Long-term travel-time perturbations for the station pair II.PFO–AZ.FRD. (a) Weekly stacked correlation functions with 2-month smoothing. The correlations are plotted every 6 weeks for visualization, and the long-term average is shown on the right. The color represents the *dt* measurements relative to the long-term average. (b) Ten-year *dt* measurements and wavelet coherence. The black dashed lines show the linear regressions before and after the travel-time offset in early 2014.

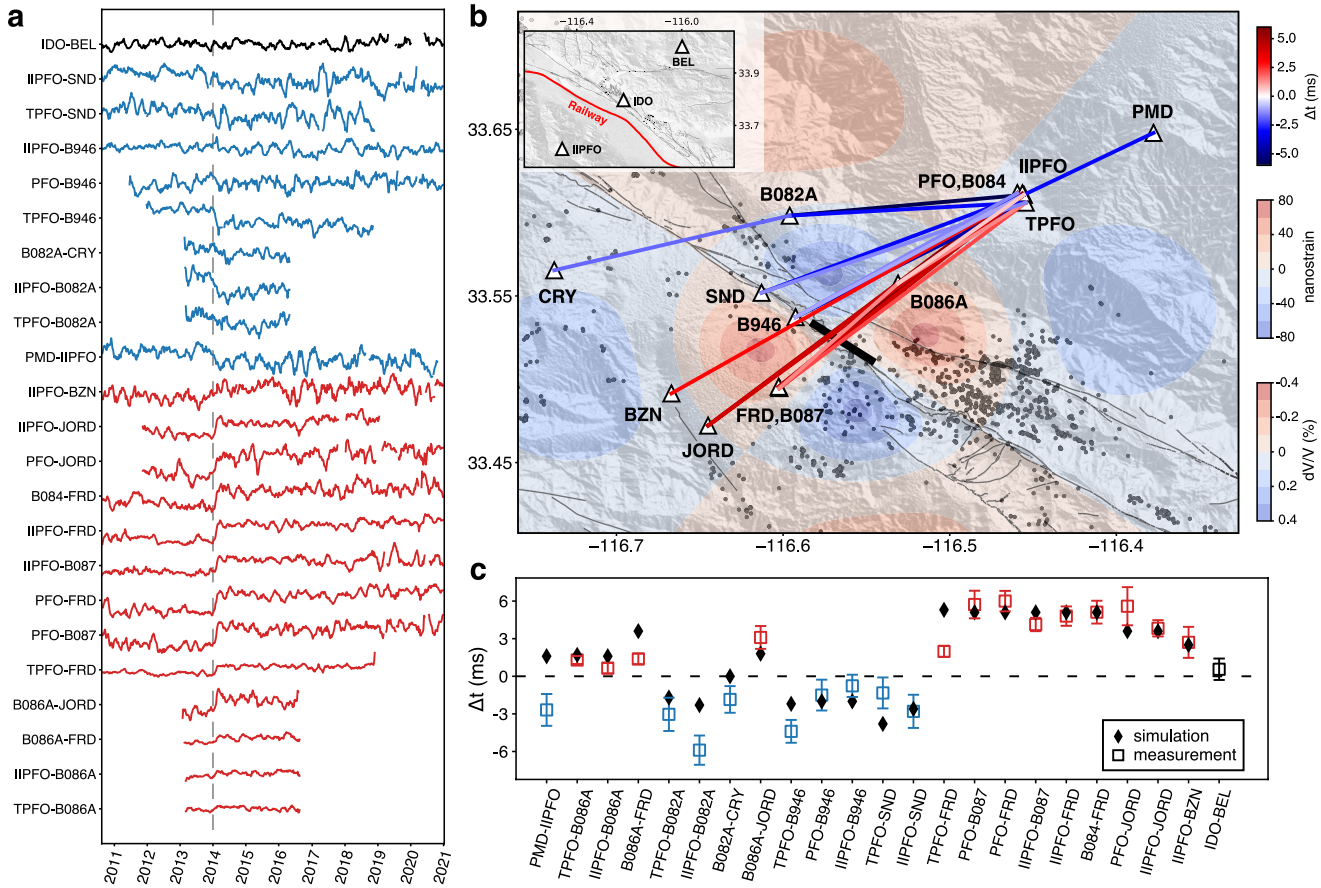

Figure 3. Travel-time shift measurements. (a) Long-term *dt* measurements for all of the considered station pairs. Pairs with positive (negative) Δt are shown in red (blue). The reference station pair IDO–BEL is shown in black. (b) Map of the station pairing for the measured Δt. The background colors indicate the volumetric strain at 1 km in depth from the preferred dislocation model (Table 1), with dilatational (compressional) strain in red (blue). The relative velocity change $\boldsymbol{dV/V}$ is calculated from the volumetric strain (Text S2 in Supporting Information S1). The thick black line marks the surface projection of the dislocation, and local earthquakes (Ross et al., 2019) during the 2-month velocity-change period are shown as black dots. The inset in the top left corner shows station II.PFO, CI.IDO, and CI.BEL. (c) Measured and simulated Δt values, using the same colors as in (a).

3. Possible Interpretation

The spatial distribution of Δt suggests a complicated pattern of velocity changes. Opening and closing voids or cracks can modulate the speed of compressional waves and yield either velocity decreases or increases (Walsh, 1965). Previous studies have argued for the existence of deep aseismic slip at the Anza seismic gap (Inbal et al., 2017; Wdowinski, 2009) and post-seismic slip at nearby seismically active regions (Shaddox et al., 2021). Aseismic transients are also predicted at the bottom of the seismogenic zone in earthquake cycle simulations, with a proposed transition of heterogeneous frictional properties below the locking depth provided to explain the deep extent of the seismicity (Jiang & Fialko, 2016).

We search for a simple dislocation model to explain our velocity-change observations and assess if they could have been caused by an aseismic slip. We use the Coulomb software (Lin & Stein, 2004) to simulate volumetric strain from an aseismic transient and convert the strain to seismic velocity change ($\boldsymbol{dV/V}$) through depth-dependant velocity-stress sensitivity (Text S2 in Supporting Information S1). The modeled $\boldsymbol{dV/V}$ is then converted to travel-time differences using full-waveform simulations of correlation functions (Sager et al., 2022) with and without velocity perturbations (Text S2 in Supporting Information S1). The travel-time differences measured from the simulated correlation functions are compared with the observations to adjust the dislocation model. To simplify the simulation, we assume a pure vertical slip patch rupturing along strike and fix the aspect

ratio (length/width) as 2, which is reported as the medium value for SSEs at Parkfield (Tan & Marsan, 2020). The Δt polarity constrains the position of the slip patch close to the edge of the seismic gap. We perform a grid search over the center, the depth, the length, and the size of the slip. Each of the first three parameters varies at a 2-km interval, and the slip size is chosen from 0.1, 0.2 to 0.4 m. The weighted summation of the misfit between simulations and observations is used to choose the ultimate model, with the inverse values of Δt uncertainties used as the weights. The simulated Δt values from the preferred model (Table 1) are presented against the observations in Figure 3c.

Given the simplified velocity model, the assumed uniform elastic properties in the strain simulation, and the considerable uncertainty of the stress-velocity sensitivity, finding the best dislocation model is nontrivial. Nevertheless, the simulated travel-time changes from the preferred dislocation model fit the observations reasonably well in both polarity and amplitude (Figure 3c). The modeled slip is 0.2 m, and the equivalent moment magnitude is 5.1. This moment magnitude is slightly below the Global Positioning System detection threshold, estimated to be 5.2 (Figure 4; Text S3 in Supporting Information S1). We do not observe clear signals on strainmeters close to the fault. However, after the corrections for offsets, tidal strains, barometric pressure variations, and long-term borehole trends, month-long strain fluctuations still present and dominate the strain measurements (Figure S8 in Supporting Information S1). The simulated volumetric strains at nearby strainmeters are of the order of 10 nanostrain, much smaller than the fluctuations. Such small magnitudes possibly explain the lack of related observations from standard geophysical methods.

4. Discussion and Conclusion

Unlike subduction SSEs accompanied by abundant seismic activity (Beroza & Ide, 2011), only a few earthquakes occurred in the vicinity of the inverted SSE during the 2-month period (Figure 5). The majority of these earthquakes appear as a swarm at a depth of 8.8 km. The general quiescence around the slipped patch suggests that this earthquake swarm was likely triggered. The lack of seismicity in the vicinity of the SSE is not surprising, given the locked nature of the fault segment (Sanders & Kanamori, 1984). Inbal et al. (2017) also reported similar findings for deep aseismic transients in the same region. SSEs at strike-slip faults are often not accompanied by tectonic tremors (Rousset et al., 2016), probably due to the different rheology and conditions compared to subduction zones. Inbal et al. (2017) observed an increasing seismicity rate in the Hot Springs and Trifurcation region associated with deep aseismic transients. They explained the rate increase as the result of creep-induced fault loading. We also observe an elevated seismicity rate at the beginning of 2014, especially in the Trifurcation area (Figure S9B in Supporting Information S1); however, whether this change is related to the modeled aseismic slip requires further investigations.

The preferred dislocation model is at the bottom of the locked fault section (Lindsey et al., 2014), consistent with a transition zone between seismogenic velocity-weakening and deeper velocity-strengthening regions. Such mechanical heterogeneity can reflect a complex structure (Jiang & Fialko, 2016) or spatially variable pore pressure suggested by fluid-driven swarms (Ross & Cochran, 2021). The modeled SSE is also located at the southern end of the seismic gap, at the transition to the zone with high seismic activity, indicating possible lateral variations of mechanical properties. The modeled SSE had a stress drop of a few hundred kPa, in the upper range for SSEs (Bartlow et al., 2014). The resulting positive Coulomb stress change in the seismic gap is significant enough to trigger a large earthquake (Radiguet et al., 2016). It is worth noting that we do not observe appreciable travel-time perturbations associated with local moderate-sized earthquakes (Ross et al., 2019), which are accompanied by aseismic slip revealed by strainmeter data and near-repeating

Table 1
Preferred Dislocation Parameters

Starting latitude	Starting longitude	Ending latitude	Ending longitude	Depth (km)	Right lateral slip (cm)	Dip (°)	Rake (°)
33.5113	−116.5470	33.5330	−116.5814	6–8	20	90	180

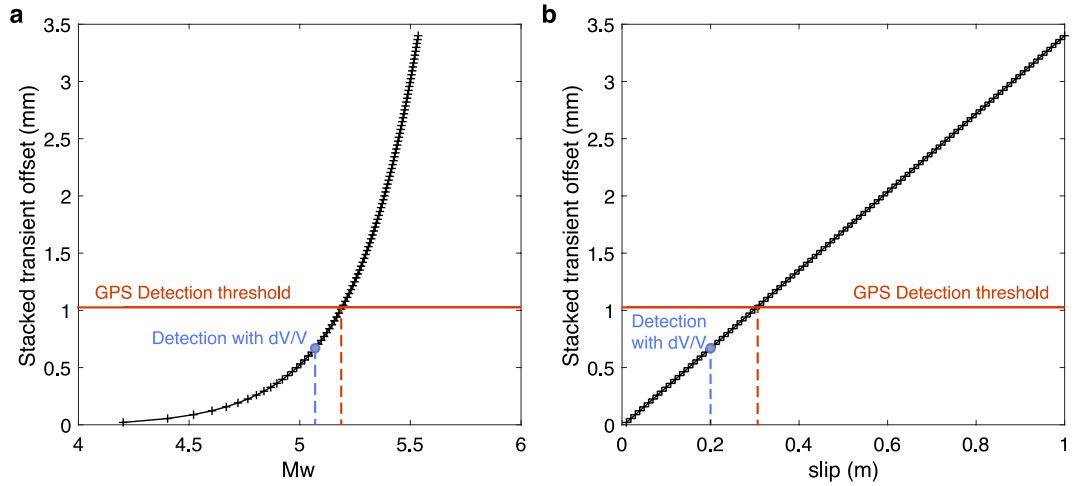

Figure 4. Minimum detection threshold with the current GPS network. Predicted GPS stacked offsets for a slip on the dislocation found with the *dt* analysis as a function of magnitude (a) and slip (b). The red lines indicate the detection thresholds with the current GPS network. The blues dots indicate the estimated magnitude and slip from the *dt* analysis.

earthquakes (Shaddox et al., 2021). Simulations for the M4.7 March 2013 Anza Earthquake (Figure S10 in Supporting Information S1) show that the induced strain has smaller amplitudes than the SSE and negligible travel-time changes. The strongly affected region is also further away from the sensitivity zone of the reconstructed interferometric body waves.

We observe a complicated pattern of seismic velocity change and interpret it as a result of an SSE at depth. Despite other possible explanations, the source of change should not be shallow, given the body-wave sensitivity. Detecting hidden fault movements significantly improves the understanding of the interaction between aseismic and seismic slips, a necessary step to characterize large earthquakes' preparation phase. The presented methodology and results rely on freight trains as seismic sources; however, other opportune sources, for example, car/truck traffic and industrial activities, could also be used after careful examinations of source signatures. Using anthropogenic seismic signals opens up new possibilities for monitoring geological targets of interest, such as fault systems, volcanoes, and geothermal or carbon storage reservoirs.

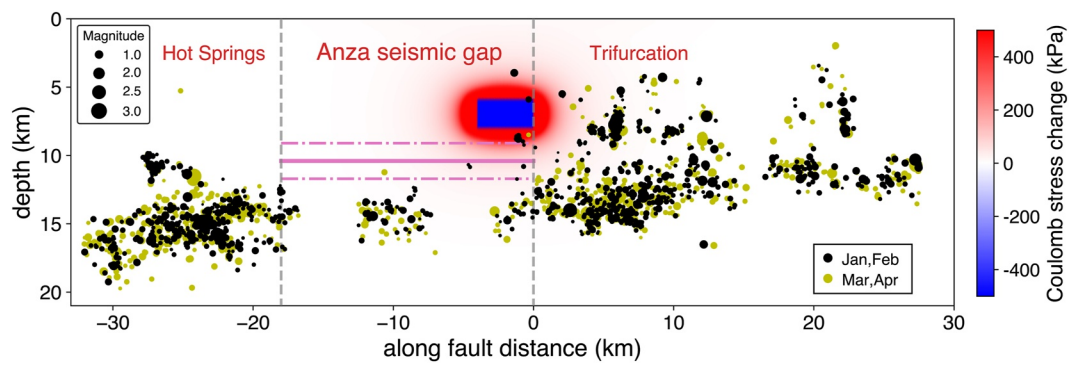

Figure 5. The along-fault cross-section of Coulomb stress changes from the dislocation slip model and the earthquakes within 3 km of the fault zone. Earthquakes in January and February 2014 are shown in black, and those in March and April 2014 are yellow. The number of earthquakes surrounding the dislocation dropped significantly after the slip (Figure S9A in Supporting Information S1). The solid magenta line represents the geodetic locking depth (Lindsey et al., 2014), and the dashed lines mark its uncertainty.

Data Availability Statement

All the seismic waveform data used can be accessed through IRIS. The networks include the ANZA Seismic Network (https://doi.org/10.7914/SN/AZ), the Southern California Seismic Network (https://doi.org/10.7914/SN/CI), the 2018 FaultScan dense array network (https://doi.org/10.7914/SN/9K_2018), and the Plate Boundary Observatory Borehole Seismic Network (no DOI available at present, but the information could be accessed through https://www.fdsn.org/networks/detail/PB/). The processed borehole strainmeter data (https://www.unavco.org/data/strain-seismic/bsm-data/bsm-data.html) and Global Positioning System data (https://www.unavco.org/data/gps-gnss/gps-gnss.html) were obtained from UNAVCO (https://www.unavco.org). We use pycorr software package (https://doi.org/10.5281/zenodo.6793401) to download the continuous seismic data and perform seismic interferometry. The dt measurement is calculated using the wavelet method (https://doi.org/10.5281/zenodo.4783514); the Coulomb 3 software is used for the strain simulation (https://www.usgs.gov/node/279387); the full-waveform simulation of the correlation wavefield is developed based on the Salvus package (https://mondaic.com), and the script for this study can be found at https://doi.org/10.5281/zenodo.6792393.

Acknowledgments

We thank numerous researchers for constructive discussions at different stages of this study. These include Michel Campillo, Nikolai Shapiro, Gregory Beroza, William Ellsworth, Zack Ross, Anne Socquet, Mathilde Radiguet, and Jean-Paul Ampuero. This study was funded by the European Research Council (ERC) under Grant Agreement Number 817803 (FAULTSCAN) and 742335 (F-IMAGE). Y.B.Z. acknowledges support from the U.S. Department of Energy (award DE-SC0016520). The paper benefitted from useful comments by Editor Germán Prieto, Tim Clements and two anonymous referees.

References

Bartlow, N. M., Wallace, L. M., Beavan, R. J., Bannister, S., & Segall, P. (2014). Time-dependent modeling of slow slip events and associated seismicity and tremor at the Hikurangi subduction zone, New Zealand. *Journal of Geophysical Research: Solid Earth*, *119*(1), 734–753. https://doi.org/10.1002/2013jb010609

Beroza, G. C., & Ide, S. (2011). Slow earthquakes and nonvolcanic tremor. *Annual Review of Earth and Planetary Sciences*, *39*(1), 271–296. https://doi.org/10.1146/annurev-earth-040809-152531

Brenguier, F., Boué, P., Ben-Zion, Y., Vernon, F., Johnson, C. W., Mordret, A., et al. (2019). Train traffic as a powerful noise source for monitoring active faults with seismic interferometry. *Geophysical Research Letters*, *46*(16), 9529–9536. https://doi.org/10.1029/2019gl083438

Brenguier, F., Campillo, M., Hadziioannou, C., Shapiro, N. M., Nadeau, R. M., & Larose, É. (2008). Postseismic relaxation along the San Andreas Fault at Parkfield from continuous seismological observations. *Science*, *321*(5895), 1478–1481. https://doi.org/10.1126/science.1160943

Brenguier, F., Campillo, M., Takeda, T., Aoki, Y., Shapiro, N. M., Briand, X., et al. (2014). Mapping pressurized volcanic fluids from induced crustal seismic velocity drops. *Science*, *345*(6192), 80–82. https://doi.org/10.1126/science.1254073

Clements, T., & Denolle, M. A. (2018). Tracking groundwater levels using the ambient seismic field. *Geophysical Research Letters*, *45*(13), 6459–6465. https://doi.org/10.1029/2018gl077706

Inbal, A., Ampuero, J. P., & Avouac, J. P. (2017). Locally and remotely triggered aseismic slip on the central San Jacinto Fault near Anza, CA, from joint inversion of seismicity and strainmeter data. *Journal of Geophysical Research: Solid Earth*, *122*(4), 3033–3061. https://doi.org/10.1002/2016jb013499

Inbal, A., Cristea-Platon, T., Ampuero, J. P., Hillers, G., Agnew, D., & Hough, S. E. (2018). Sources of long-range anthropogenic noise in Southern California and implications for tectonic tremor detection. *Bulletin of the Seismological Society of America*, *108*(6), 3511–3527. https://doi.org/10.1785/0120180130

Jiang, J., & Fialko, Y. (2016). Reconciling seismicity and geodetic locking depths on the Anza section of the San Jacinto Fault. *Geophysical Research Letters*, *43*(20), 10–663. https://doi.org/10.1002/2016gl071113

Johnson, H. O., Agnew, D. C., & Wyatt, F. K. (1994). Present-day crustal deformation in southern California. *Journal of Geophysical Research*, *99*(B12), 23951–23974. https://doi.org/10.1029/94jb01902

Kato, A., & Ben-Zion, Y. (2021). The generation of large earthquakes. *Nature Reviews Earth & Environment*, *2*(1), 26–39. https://doi.org/10.1038/s43017-020-00108-w

Lin, J., & Stein, R. S. (2004). Stress triggering in thrust and subduction earthquakes and stress interaction between the southern San Andreas and nearby thrust and strike-slip faults. *Journal of Geophysical Research*, *109*(B2). https://doi.org/10.1029/2003jb002607

Lindsey, E. O., Sahakian, V. J., Fialko, Y., Bock, Y., Barbot, S., & Rockwell, T. K. (2014). Interseismic strain localization in the San Jacinto Fault zone. *Pure and Applied Geophysics*, *171*(11), 2937–2954. https://doi.org/10.1007/s00024-013-0753-z

Niu, F., Silver, P. G., Daley, T. M., Cheng, X., & Majer, E. L. (2008). Preseismic velocity changes observed from active source monitoring at the Parkfield SAFOD drill site. *Nature*, *454*(7201), 204–208. https://doi.org/10.1038/nature07111

Peng, Z., & Gomberg, J. (2010). An integrated perspective of the continuum between earthquakes and slow-slip phenomena. *Nature Geoscience*, *3*(9), 599–607. https://doi.org/10.1038/ngeo940

Pinzon-Rincon, L., Lavoué, F., Mordret, A., Boué, P., Brenguier, F., Dales, P., et al. (2021). Humming trains in seismology: An opportune source for probing the shallow crust. *Seismological Research Letters*, *92*(2A), 623–635. https://doi.org/10.1785/0220200248

Radiguet, M., Perfettini, H., Cotte, N., Gualandi, A., Valette, B., Kostoglodov, V., et al. (2016). Triggering of the 2014 Mw7. 3 Papanoa earthquake by a slow slip event in Guerrero, Mexico. *Nature Geoscience*, *9*(11), 829–833. https://doi.org/10.1038/ngeo2817

Rockwell, T. K., Dawson, T. E., Young Ben-Horin, J., & Seitz, G. (2015). A 21-event, 4,000-year history of surface ruptures in the Anza seismic gap, San Jacinto Fault, and implications for long-term earthquake production on a major plate boundary fault. *Pure and Applied Geophysics*, *172*(5), 1143–1165. https://doi.org/10.1007/s00024-014-0955-z

Ross, Z. E., & Cochran, E. S. (2021). Evidence for latent crustal fluid injection transients in Southern California from long-duration earthquake swarms. *Geophysical Research Letters*, *48*(12), e2021GL092465. https://doi.org/10.1029/2021gl092465

Ross, Z. E., Trugman, D. T., Hauksson, E., & Shearer, P. M. (2019). Searching for hidden earthquakes in Southern California. *Science*, *364*(6442), 767–771. https://doi.org/10.1126/science.aaw6888

Rousset, B., Jolivet, R., Simons, M., Lasserre, C., Riel, B., Milillo, P., et al. (2016). An aseismic slip transient on the North Anatolian Fault. *Geophysical Research Letters*, *43*(7), 3254–3262. https://doi.org/10.1002/2016gl068250

Sager, K., Tsai, V. C., Sheng, Y., Brenguier, F., Boué, P., Mordret, A., & Igel, H. (2022). Modelling P waves in seismic noise correlations: Advancing fault monitoring using train traffic sources. *Geophysical Journal International*, *228*(3), 1556–1567. https://doi.org/10.1093/gji/ggab389

Sanders, C. O., & Kanamori, H. (1984). A seismotectonic analysis of the Anza seismic gap, San Jacinto Fault zone, southern California. *Journal of Geophysical Research*, *89*(B7), 5873–5890. https://doi.org/10.1029/jb089ib07p05873

Shaddox, H. R., Schwartz, S. Y., & Bartlow, N. M. (2021). Afterslip and spontaneous aseismic slip on the Anza segment of the San Jacinto Fault Zone, Southern California. *Journal of Geophysical Research: Solid Earth*, *126*(6), e2020JB020460. https://doi.org/10.1029/2020jb020460

Tan, Y. J., & Marsan, D. (2020). Connecting a broad spectrum of transient slip on the San Andreas fault. *Science Advances*, *6*(33), eabb2489. https://doi.org/10.1126/sciadv.abb2489

Walsh, J. B. (1965). The effect of cracks on the compressibility of rock. *Journal of Geophysical Research*, *70*(2), 381–389. https://doi.org/10.1029/jz070i002p00381

Wdowinski, S. (2009). Deep creep as a cause for the excess seismicity along the San Jacinto Fault. *Nature Geoscience*, *2*(12), 882–885. https://doi.org/10.1038/ngeo684

References From the Supporting Information

Ayala-Garcia, D., Curtis, A., & Branicki, M. (2021). Seismic interferometry from correlated noise sources. *Remote Sensing*, *13*(14), 2703. https://doi.org/10.3390/rs13142703

Bevis, M., & Brown, A. (2014). Trajectory models and reference frames for crustal motion geodesy. *Journal of Geodesy*, *88*(3), 283–311. https://doi.org/10.1007/s00190-013-0685-5

Fang, H., Zhang, H., Yao, H., Allam, A., Zigone, D., Ben-Zion, Y., et al. (2016). A new algorithm for three-dimensional joint inversion of body wave and surface wave data and its application to the Southern California plate boundary region. *Journal of Geophysical Research: Solid Earth*, *121*(5), 3557–3569. https://doi.org/10.1002/2015jb012702

Herring, T. A., Melbourne, T. I., Murray, M. H., Floyd, M. A., Szeliga, W. M., King, R. W., et al. (2016). Plate boundary observatory and related networks: GPS data analysis methods and geodetic products. *Reviews of Geophysics*, *54*(4), 759–808. https://doi.org/10.1002/2016rg000529

Lobkis, O. I., & Weaver, R. L. (2001). On the emergence of the Green's function in the correlations of a diffuse field. *Journal of the Acoustical Society of America*, *110*(6), 3011–3017. https://doi.org/10.1121/1.1417528

Mao, S., Mordret, A., Campillo, M., Fang, H., & van der Hilst, R. D. (2020). On the measurement of seismic traveltime changes in the time–frequency domain with wavelet cross-spectrum analysis. *Geophysical Journal International*, *221*(1), 550–568. https://doi.org/10.1093/gji/ggz495

Rousset, B., Bürgmann, R., & Campillo, M. (2019). Slow slip events in the roots of the San Andreas Fault. *Science Advances*, *5*(2), eaav3274. https://doi.org/10.1126/sciadv.aav3274

Silver, P. G., Daley, T. M., Niu, F., & Majer, E. L. (2007). Active source monitoring of cross-well seismic travel time for stress-induced changes. *Bulletin of the Seismological Society of America*, *97*(1B), 281–293. https://doi.org/10.1785/0120060120

Tromp, J., Luo, Y., Hanasoge, S., & Peter, D. (2010). Noise cross-correlation sensitivity kernels. *Geophysical Journal International*, *183*(2), 791–819. https://doi.org/10.1111/j.1365-246x.2010.04721.x

Yamamura, K., Sano, O., Utada, H., Takei, Y., Nakao, S., & Fukao, Y. (2003). Long-term observation of in situ seismic velocity and attenuation. *Journal of Geophysical Research*, *108*(B6). https://doi.org/10.1029/2002jb002005